AIAA JOURNAL
Vol. 43, No. 4, April 2005

Autonomous Control of Micro Aircraft Vehicles Falling Through an Atmospheric Boundary Layer

A. J. Dorgan,* E. Loth,† and E. Frazzoli‡
University of Illinois at Urbana–Champaign, Urbana, Illinois 61801-2935

A trajectory control problem for simple micro air vehicles (MAVs) is introduced and studied. The MAVs are endowed with the ability to estimate their position and velocity and can control their drag coefficient. The objective of this work is to design a control law for the drag coefficient in order to land the MAV close to a desired streamwise location, after being dropped from an airborne carrier at low altitude. We use a simple model-predictive control law, relying on a two-dimensional time-averaged atmospheric velocity field, which is validated on an unsteady three-dimensional representation of an unstratified atmospheric boundary layer. The simulation results show that the proposed control law results in a significant (10-fold) improvement in the accuracy of the streamwise landing point location, with respect to the uncontrolled case. Similar results are obtained when errors are considered in the location of the release point and in the estimate of the mean flowfield.

I. Introduction

As the miniaturization of electronic components (including computation and communication devices) progresses at a fast pace, there is an increasing interest and opportunity for the development of pervasive, sensor-rich networks.[1] A typical objective of such networks is the monitoring of spatially localized quantities associated with a broad set of environmental and physical phenomena. The key perceived advantage of modern technologies in this context is the capability of quickly deploying affordable, efficient, scalable, and reconfigurable networks, communicating in a wireless and unsupervised fashion among themselves and with a main control station responsible for data processing and dissemination to the users.[2–4]

For example, ad hoc sensor networks can be used to detect the presence, concentration, and spatial distribution of radioactive, biological, or chemical contaminants, or to monitor the traffic of vehicles and personnel at a site of tactical interest. In these cases, one would wish for a sensor network to be placed (in the air or on the ground) in a very short time and with minimal human supervision in order to rapidly provide time-critical information. Current sensor networks rely on the careful manual deployment of sensors to achieve area coverage. However, in many foreseeable, time-critical applications, embedded devices would be deployed in an unattended way (e.g., by dropping sensors from an airplane); the lack of geometric optimization is compensated through redundancy of the network. In contrast, if the geometric deployment of the system can be controlled, better utilization of the available resources is attained (e.g., requiring a lower number of sensors to cover a given area, or allowing the coverage of a wider area given a fixed number of sensors). The problem of self-deployment of sensor networks has been explored recently.[5–7] However, the techniques introduced in the literature to date require the sensors to be endowed with sophisticated navigation and locomotion systems, granting them the ability to accurately control their own position. The problem of self-deployment of networks of simple devices, in a realistic environment subject to significant disturbances from the environment, has not been explored.

The present work is a first step in this direction. In particular, we consider the problem of self-deployment for a number of cheap, airborne sensors, with a limited ability to control their own motion. For small vehicles (spans on the order of tens of centimeters and masses on the order of tens of grams), one must consider the effect of the atmospheric boundary layer on the vehicle trajectory. For such small vehicles, the presence of wind (which is turbulent and largely unpredictable) adds a convective, effectively random, dispersive effect that can deleteriously affect the intended vehicle landing point if ignored.

The most common class of micro air vehicles (MAVs) include a propulsion system for thrust and can be used to achieve accurate trajectory control. However, this class can be severely limited in terms of range and duration as a result of the energy storage limit associated with small vehicle scales. If we consider a second class of MAVs, ones that do not carry onboard propulsion, substantial reductions in weight, size, and complexity are obtained; all of which can substantially reduce cost of such a system and/or allow more allotment of power and space to the sensor devices. For unpowered MAVs, the network can be released above the intended target with a conventional aircraft in order to eliminate the need for the MAV to transport itself to the general target area. After deployment, control of the aerodynamic lift and/or drag of these vehicles can be used to achieve the desired trajectory and landing location. Such vehicles are essentially gliders (e.g., a sailplane) when lift dominates, terminal-velocity vehicles (e.g., a parachute) when drag dominates, or hybrids (e.g., a parasail) when both lift and drag are important in determining the trajectory. In the present case of no lift (a terminal-velocity vehicle), the MAV design can be simple allowing focus on the atmospheric interaction control. In this study, we will consider autonomous control of the terminal-velocity class of vehicles with respect to landing close to a prespecified streamwise landing location. In particular, the coupling of the turbulence in the atmospheric boundary layer with the dynamic behavior of airborne microvehicles is investigated.

II. Methodology

A. Terminal-Velocity Microvehicle

To investigate possible autonomous control systems capable of controlling the deployment of a sensor network of the type just described, a scenario was considered in which a large number of microvehicles (1000) are released into a turbulent boundary layer with a freestream velocity of 10 m/s. The vehicles are deployed upstream of the target site by a full-scale or meso-scale aircraft (see Fig. 1). This concept of release allows gravity and atmospheric convection

Presented as Paper 2004-0539 at the 42nd Aerospace Sciences Meeting, Reno, NV, 5–8 January 2004; received 28 June 2004; revision received 11 October 2004; accepted for publication 12 October 2004.

*Research Assistant, Department of Aerospace Engineering. Member AIAA.

†Professor of Aerospace Engineering, Department of Aerospace Engineering, 306 Talbot Laboratory, 104 South Wright Street; loth@uiuc.edu. Associate Fellow AIAA.

‡Assistant Professor, Department of Aerospace Engineering; currently Assistant Professor of Mechanical and Aerospace Engineering, 37-138 Engineering IV, University of California, Los Angeles, 420 Westwood Plaza, Los Angeles, CA 90095; frazzoli@ucla.edu. Member AIAA.

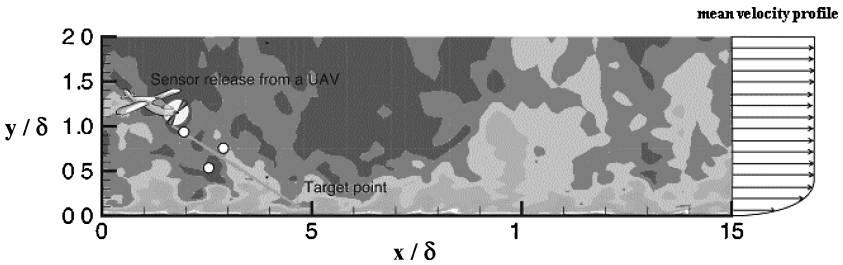

Fig. 1 Schematic of sensors (MAVs) being released from a UAV within an atmospheric boundary layer (contours denote instantaneous streamwise velocity).

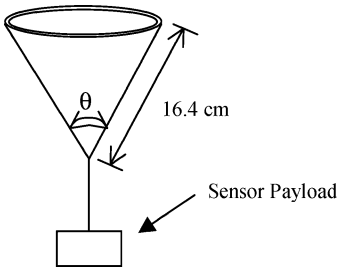

Fig. 2 Schematic showing the configuration of the MAV, where the expansion angle θ can vary from 10 to 80 deg.

to be exploited in transporting the vehicles to the target area. For the present study, a single goal of landing on the preassigned streamwise target location was imposed (i.e., the target is simply a line along the ground normal to the freestream flow). Landing in the vicinity of the target is achieved by controlling each vehicle's terminal velocity.

Although the methodology and results discussed herein are applicable to any MAV that can control its terminal velocity, the basic concept the authors have in mind is a downward-pointing conical structure (used for controlling the drag), as shown in Fig. 2. The sensor payload could be slung beneath the vehicle and would provide stability of the structure's orientation. This concept is similar to the pyramid shaped vehicles built by Zussman et al.,[8] shown in Fig. 3. A total vehicle mass of 30 g was assumed for all of the results presented herein. This was based on a reasonable minimum mass for a craft that only carried microsensors, a micro global positioning system device, and microcommunications. To allow for a large range of terminal velocities, the vehicle can vary its cone vertex angle θ as shown in Fig. 2. The vertex angle is chosen as the control input and is allowed to vary from 10 to 80 deg. Thus, the vehicles will be capable of trajectory modification via changes in the terminal velocity with only modest expenditures of energy.

The slant height of the cone was chosen as 16.7 cm with a nominal vertex angle of 45 deg to give a vehicle a terminal velocity of 4 m/s in the nominal configuration. A far-surface wind speed of 10 m/s was assumed, which results in a friction velocity of 0.6 m/s for the present direct numerical simulation of a zero-stratification turbulent boundary layer. Thus, the ratio of the vehicle's baseline terminal velocity to the friction velocity is 6.7 for the assumed craft size and wind conditions, but significantly lower and higher values are possible.

B. Simulation of the Atmospheric Boundary Layer

The physical atmospheric boundary layer (ABL) flows over the Earth's surface, which influences the thickness and spatial growth of the layer, in such a way that a typical ABL extends roughly 300 m above ground level. Such a flowfield is illustrated in Fig. 1 for the MAV release, where the spatial coordinates are scaled by the reference boundary-layer thickness.

Because the ABL is turbulent, a time-averaged description does not account for all of the velocity fluctuations and turbulent dispersion. To model the three-dimensional unsteady motion, a direct numerical simulation (DNS) of the incompressible Navier–Stokes equations is employed for $Re_\tau = 270$, where Re_τ is the Reynolds number based on the boundary-layer thickness and u_τ is the wall friction velocity (based on the shear stress). Because DNS does not require empirical modeling for the turbulence, this seemingly modest Reynolds number (by atmospheric standards) requires very large CPU resources. However, the variation caused by Reynolds number in a turbulent boundary layer is generally weak enough so that the DNS will give a reasonable representation of the ABL. Zero-density stratification is assumed (consistent with a neutrally stable ABL), as this assumption substantially simplified the computations, though it should be recognized that the turbulence levels will be modified if a stable or unstable density distribution were imposed.

The DNS boundary-layer code used herein was developed by Spalart and Watmuff[9] to simulate a three-dimensional spatially developing turbulent boundary layer, which is ergodically stationary in time. The DNS solution is spectrally accurate in the three spatial directions and second-order accurate in time. The solution domain is discretized by 256 nodes in the stream direction, 96 in the span direction, and 55 in the vertical direction. (Further details are available in Dorgan and Loth.[10]) The two-dimensional mean streamwise fluid velocity field $[u_f(x, y)]$ is shown in Fig. 4, where $[\cdots]$ is a long time average over all spanwise locations. The nondimensional profiles of mean streamwise velocity u and turbulent kinetic energy k taken at a typical streamwise station are shown in Fig. 5 in terms of $y^+ = yu_\tau/\nu$ (where ν is the kinematic viscosity). In Fig. 5a, the mean streamwise velocity profile yields a viscous sublayer below $y^+ \sim 10$, and the boundary-layer edge is seen at roughly $y^+ = 270$—corresponding to the reference boundary-layer thickness δ. The common law of the wall and log-law expressions are included for comparison with high-Reynolds-number boundary layers. The departure from the typical log-layer behavior is typical of DNS and is attributed to the low Reynolds number of the simulation. Figure 5b shows the turbulent kinetic energy profile, which is based on the three velocity autocorrelations, that is, $k = [u_i' u_i']/2$, where the repeated subscript i denotes summation over the three velocity components and the prime denotes a fluctuation about the mean. Below $y^+ = 1$, the energy is nearly zero and approaches a maximum at around $y^+ = 10$ before returning to zero toward the boundary-layer edge and is similar to the results of Klebanov, reported by Hinze,[11] for $Re_\tau = 2.8 \times 10^3$.

C. Simulation of the Vehicle Trajectories

The MAVs are modeled as rigid bodies of finite adjustable drag and zero lift (i.e., no lifting surfaces are included) with densities much greater than that of the surrounding continuum. Therefore, a Lagrangian equation of motion is employed herein and has the following form:

$$m_v \frac{\mathrm{d}u_{v_i}}{\mathrm{d}t} = F_{D_i} + F_{G_i} \tag{1}$$

where m_v is the vehicle mass, F_D is the steady-state drag force, F_G is the gravitational force, and i indicates the directional components. These assumptions can be reasonable if the MAVs are simply sensor-carrying devices with little aerodynamic construction. Applying point force formulations,[12] the vehicle-aerodynamic forces for this study are summarized as

$$F_{D_i} = -\tfrac{1}{2}\rho_f V_{\mathrm{rel}} \left(V_{\mathrm{rel}_i}\right)(C_D A)_i \tag{2}$$

$$F_{G_i} = m_v g_i \tag{3}$$

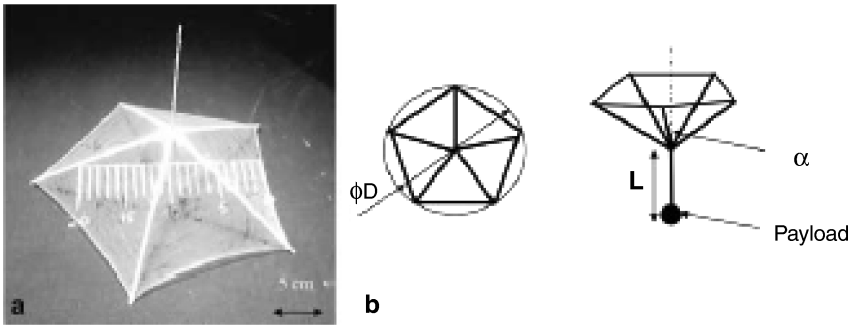

Fig. 3 Figure from Zussman et al.[8] showing their pyramid shaped vehicles: a) an actual vehicle with ∼25-cm maximum dimension and b) schematic of a general vehicle.

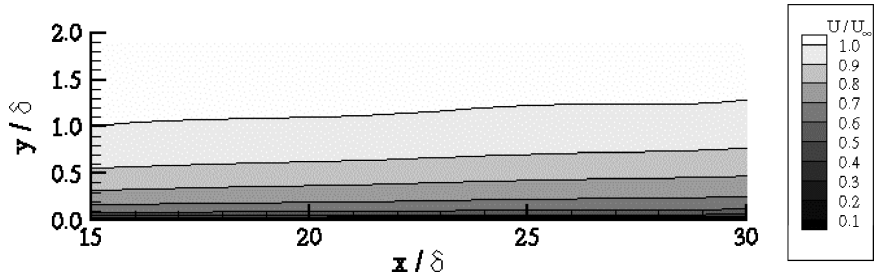

Fig. 4 DNS statistics for the two-dimensional mean velocity field normalized by the freestream conditions. (Contours denote mean streamwise velocity.)

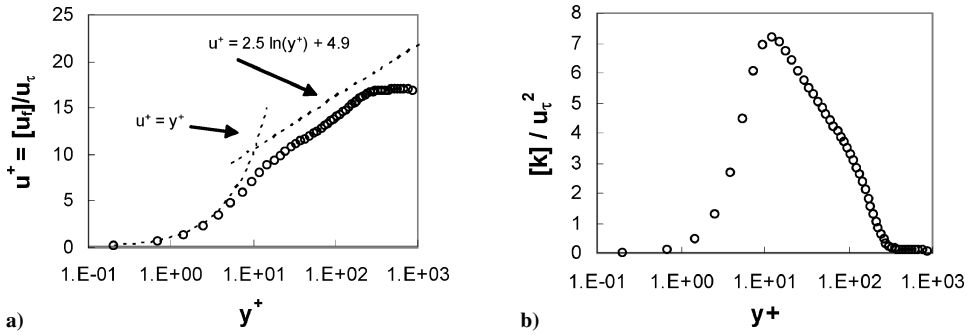

Fig. 5 DNS statistics for a) the mean velocity profile normalized by u_τ and b) the turbulent kinetic energy profile a normalized by u_τ^2.

where $V_{\text{rel}_i} = u_{v_i} - u_{f_i}$ with subscripts v and f distinguishing vehicle velocities from fluid velocities and V_{rel} is the magnitude of the relative velocity vector (which is equal to the terminal vehicle velocity V_{term} in quiescent conditions). As the vehicle is modeled as a conical structure, the drag coefficient will be anisotropic, that is, the drag coefficients along and perpendicular to the axis of symmetry will be different. The C_D for a cone along the line of symmetry is available in White[13] for a variety of cone angles and was thus used for the vertical direction. Perpendicularly, the cone drag coefficient is not well known so that a C_D appropriate for a cylinder that has the same surface area as the cone[13] is used for the horizontal directions. In both cases, this assumes the axis of symmetry of the cone is aligned with the gravity vector, which is reasonable because the payload (sensor package) is assumed to be heavy enough to keep the vehicle in this configuration.

In the present study, groups of 50 vehicles evenly distributed across the span of the domain were released every other time step in the freestream flow at the mean boundary-layer edge δ and at a streamwise location of $\Lambda_x/3$. This process was continued until a total of 1000 vehicles had been released in the simulation. In all cases, the vehicle's objective was to reach a static streamwise target set on the ground x_{target} located downstream of the release location (a schematic is shown in Fig. 6).

The vehicles are released into the three-dimensional unsteady simulation with the vector sum of the mean velocity and the terminal velocity for initial conditions, that is,

$$u_{\text{vi}} = [u_{\text{fi}}] + V_{\text{termi}} \tag{4}$$

such that the streamwise injection velocity is caused by the mean fluid velocity and there is no initial spanwise component. The vehicle trajectories are computed by integrating the equation of motion [Eq. (1)] subject to the point-force approximations [Eqs. (2) and (3)] using a Lagrangian tracking technique similar to Dorgan[14] but with a nonlinear drag.

The flowfield and the trajectories for the microvehicles were solved using the identical time-step discretizations. The integration is performed using an Adams–Bashforth, predictor-corrector method and gives second-order accuracy in time.[14] Therefore, the time step was set at the maximum of that prescribed by the DNS for accuracy and stability of the fluid solution or a hard value of approximately 10^{-2} (if normalized by u_τ^2/ν, the wall timescale of the fluid) to ensure accurate vehicle tracking.[14] This was found to be statistically sufficient for the results presented herein.

D. Control of the Vehicle Trajectories

The only parameter for altering the vehicle trajectories herein is the vehicle's drag coefficient via a change in the opening angle of the cone. However, the cone angle can drastically change the vehicle's descent trajectory because this allows for more than a factor

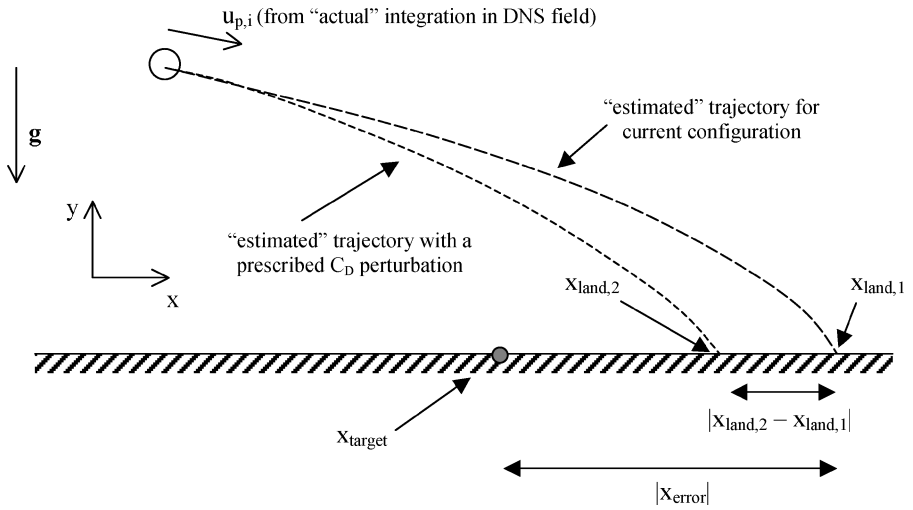

Fig. 6 Schematic illustrating the parameters used in control law (note trajectories represent integrations made in the mean flowfield).

of 10 variation in terminal velocity. In particular, the trajectory at $\theta = 80$ deg is strongly influenced by turbulent dispersion and will be dominated by the wind motion; however, at $\theta = 10$ deg the trajectory is dominated by the effects of terminal velocity, with little deflection of the trajectory due to turbulence.

The control law discussed in this paper takes the form of a nonlinear feedback on the estimated landing error. After each time step, the simulation used the vehicle's instantaneous velocity and position (obtained from the three-dimensional unsteady DNS solution) as initial conditions for integration of the vehicle equation of motion. Because it was assumed that the future flowfield was not known to the vehicle, the predicted landing location for the control law was computed using an estimated trajectory, which is based only on the two-dimensional steady flowfield. Note, this will differ from the actual trajectory, which is based on the full DNS solution. This low-cost numerical integration using the estimated trajectory is done for two craft configurations as shown in Fig. 6. The first uses the current aerodynamic configuration (i.e., current opening angle θ, which is directly related to C_D) and determines the expected error from the target location. The second configuration uses an incrementally changed θ (though with the same initial velocity and position) to estimate the correlation between the landing position and θ. Thus, the two landing sites have the following functional dependence:

$$x_{\text{land},1} = f\left(u^j_{p,i}, x^j_{p,i}, \theta\right), \qquad x_{\text{land},2} = f\left(u^j_{p,i}, x^j_{p,i}, \theta + \Delta\theta\right) \quad (5)$$

where $x_{\text{land},1}$ refers to the first shot, $x_{\text{land},2}$ represents the second shot, i indicates the directional components, and j indicates the time step of the DNS. The error in the current trajectory at time t^j is then given by

$$x^j_{\text{error}} = x_{\text{land},1} - x_{\text{target}} \quad (6)$$

and the dependency of θ on the landing position is approximated by

$$\left(\frac{\partial\theta}{\partial x_{\text{land}}}\right)^j = \frac{\Delta\theta}{x_{\text{land},2} - x_{\text{land},1}} \quad (7)$$

As such, a new θ, and thus a new C_D, can be calculated (based on the error in the trajectory and the dependency relationship) at t^j, which will land the vehicle closer to the intended target, that is,

$$\theta^{j+1} = \theta^j + \left(\frac{\partial\theta}{\partial x_{\text{land}}}\right)^j x^j_{\text{error}} \qquad \text{with} \qquad \frac{\pi}{18} \le \theta \le \frac{4\pi}{9} \quad (8)$$

and

$$C_{D,\text{cone}} = 0.6156\theta + 0.2012$$

$$C_{D,\text{cylinder}} = 0.0944\,\ell_n(1.5\tan\theta\cos\theta) + 0.6172 \quad (9)$$

based on curve fits to data given by White.[13] This procedure is continued until the vehicle lands (at $y = 0$). In the first part of the study, the control law was given exact information about the vehicle's position and the freestream velocity of the boundary layer. However, the vehicle position and wind velocity would be known to within some experimental uncertainty in actual applications or the mean wind could change over time. Thus a second set of simulations was conducted to investigate the influence of these errors in terms of the control law. The cases that imparted an error in the vehicle location simply showed that the target error increased linearly proportional to this error, for example, a 10-m error in vehicle position to the control law resulted in a 10-m deviation in the landing location, on average. As such only the velocity error studies are shown in the results section. Finally, a third set of simulations were conducted to note the effect of varying release location with a fixed downstream landing location.

III. Results

A. Single Release Study

The first study investigated the ability of the preceding control law (i.e., adaptable C_D) to improve the vehicles' streamwise landing location as compared to the uncontrolled case (i.e., fixed C_D). Figure 7 shows sample trajectories of five vehicles without control (Fig. 7a) and with control (Fig. 7b). The effect of including adaptability is quite evident, as the self-controlled vehicles all land near the target location. Figure 8 shows a comparison of controlled and uncontrolled vehicle landing locations for a release location predicted to be ideal by mean flowfield integrations (i.e., trajectory integrations considering only $[u_f]$ and $[v_f]$ and neglecting the fluctuating component predicted this release location would exactly land an uncontrolled vehicle at the specified landing location). Figure 8a shows that the landing locations of the 1000 controlled vehicles land very close to the target with little diffusion. This is in contrast to the uncontrolled vehicles (Fig. 8b), where the landing locations take on the randomly dispersed nature that is expected of turbulent particle diffusion. Not only is there a high degree of diffusion, but also a significant error in the mean location. This is not a general result, and is instead a consequence of the time chosen for release. In particular, this chosen time corresponded to a large updraft during the flight of the vehicles. Other release times could have experienced a large downdraft and a corresponding undershoot. Thus the mean velocity field is not sufficient for predicting mean trajectories if only one release time is chosen.

The improvement of vehicle performance with control can be quantified by the error in the mean landing location as well as the mean deviation about the landing location. These values were obtained and shown in Table 1 for both no control and control. For no control, a spread of about $\delta/2$ around the mean landing location

Table 1 Statistics for the single release point studies

Simulation condition	$\langle x_{\text{land}} - x_{\text{target}} \rangle / \delta$	$\langle (x_{\text{land}} - x_{\text{target}})^2 \rangle / \delta^2$
Uncontrolled	$4.07E{-}01$	$2.32E{-}01$
Controlled	$-6.83E{-}03$	$1.27E{-}04$
Controlled, but with ±10% error in mean fluid velocities	$-2.54E{-}02$	$2.61E{-}04$
Controlled, but with ±20% error in mean fluid velocities	$-1.36E{-}02$	$7.32E{-}04$
Controlled, but with ±50% error in mean fluid velocities	$2.55E{-}02$	$7.68E{-}03$

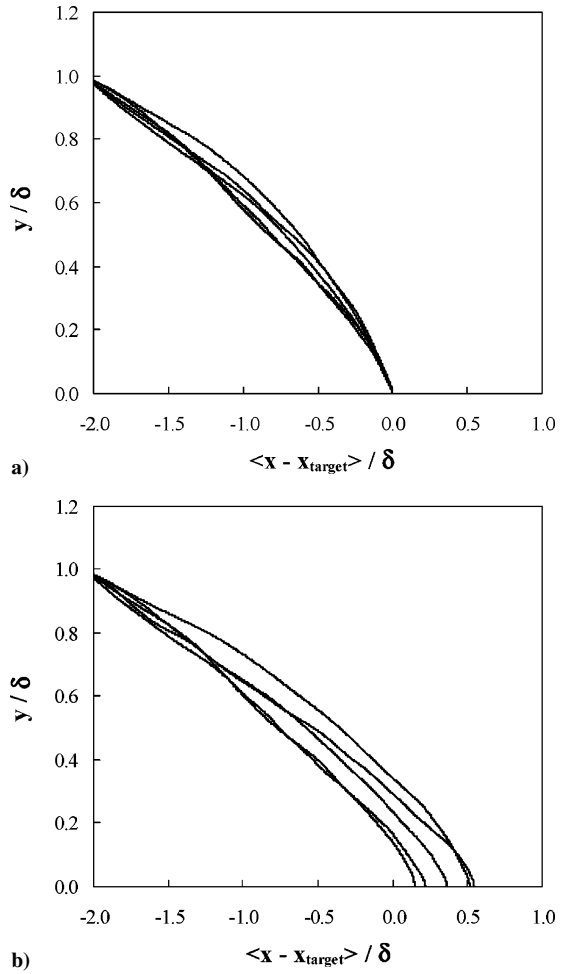

Fig. 7 Vehicle trajectories a) with and b) without control.

is seen along with a mean variance of $(\delta/2)^2$. However, the control law provides nearly 100 times more accuracy in the mean landing and 1000 times less diffusion of the vehicle cloud around the target, where $\langle \cdots \rangle$ refers to an average over all vehicles.

The preceding results can also be viewed in terms of probability distributions for landing. Figure 9a shows a discrete representation of the vehicle concentration and was taken from the data presented in Fig. 8. The vehicles' streamwise landing locations were placed into bins with a width of 0.033δ and presented here as a percent of the total vehicle cloud. The effect of the control law (with no wind error) is again quite evident as more than 80% of the vehicles landed in the bin centered on the target, which is 20 fold better than the uncontrolled case. Note that the remaining vehicles (∼20%) land only one bin upstream of the intended landing bin. Thus, the drag-modification scheme (which should require little power if physically implemented) can give good streamwise targeting accuracy. This plot also demonstrates the dispersed nature of the uncontrolled vehicles as no bin contains more than 6% of the total, with vehicles distributed over a range of about δ.

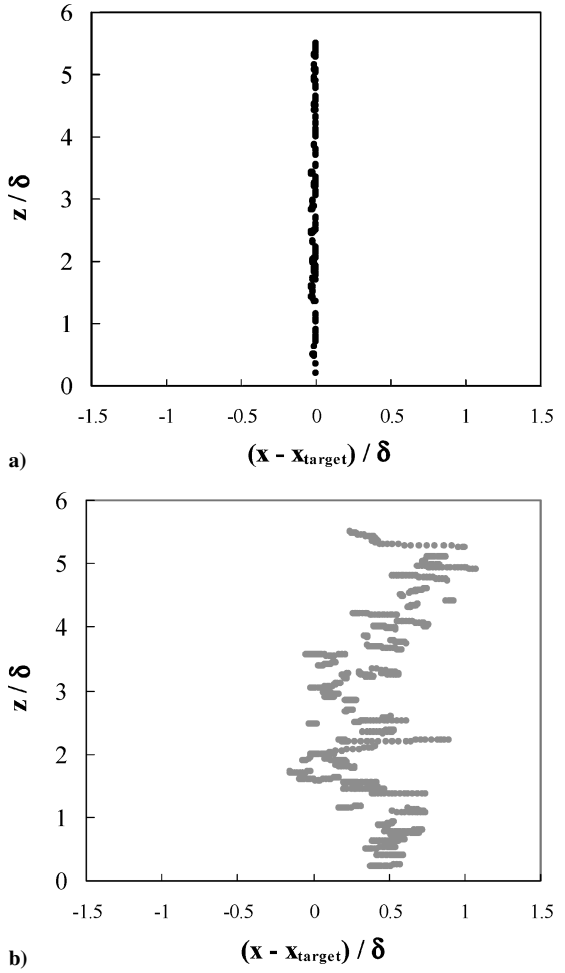

Fig. 8 Vehicle landing positions for a) controlled and b) uncontrolled simulations.

B. Tolerance of the Control Law to Estimated Wind Velocity Errors

The tolerance of the control law to errors in the fluid velocity measurements was assessed by introducing a positive and negative error in the assumed velocity of the mean field used in calculating the estimated trajectory. As in the preceding study, the vehicles were allowed precise and accurate knowledge of their position. A total of six simulations were conducted with positive and negative 10, 20, and 50% errors in the mean velocity field. The results for a particular positive and negative error (e.g., +10 and −10%) were averaged together to represent the ability of the control law to tolerate errors associated with that particular error range (e.g., ±10%). Thus, the study considered three error ranges: ±10, ±20, and ±50%, representing increasing levels of potential uncertainty in the mean fluid velocity. These averaged results are presented in Table 1. One notes an increase in landing location deviation and variance with an increase in wind velocity error, as expected. However, the controlled case was consistently more successful, that is, an order of magnitude better even with wind velocity uncertainties of ±50%. The probability distribution comparison of the controlled cases with various errors in the mean velocity field for the estimated trajectory is given as Figs. 9b–9d.

C. Influence of Release Location

In the results discussed earlier, the streamwise release location was fixed with respect to the target landing location. The distance between these two locations was consistent with the vehicle's baseline terminal velocity and the exact mean wind velocity. However, it might often be the case that the release location is not optimized or the target location changes after the release. In this case it is important to understand the sensitivity of the control law to variations in the release location. To consider this, a range of streamwise release

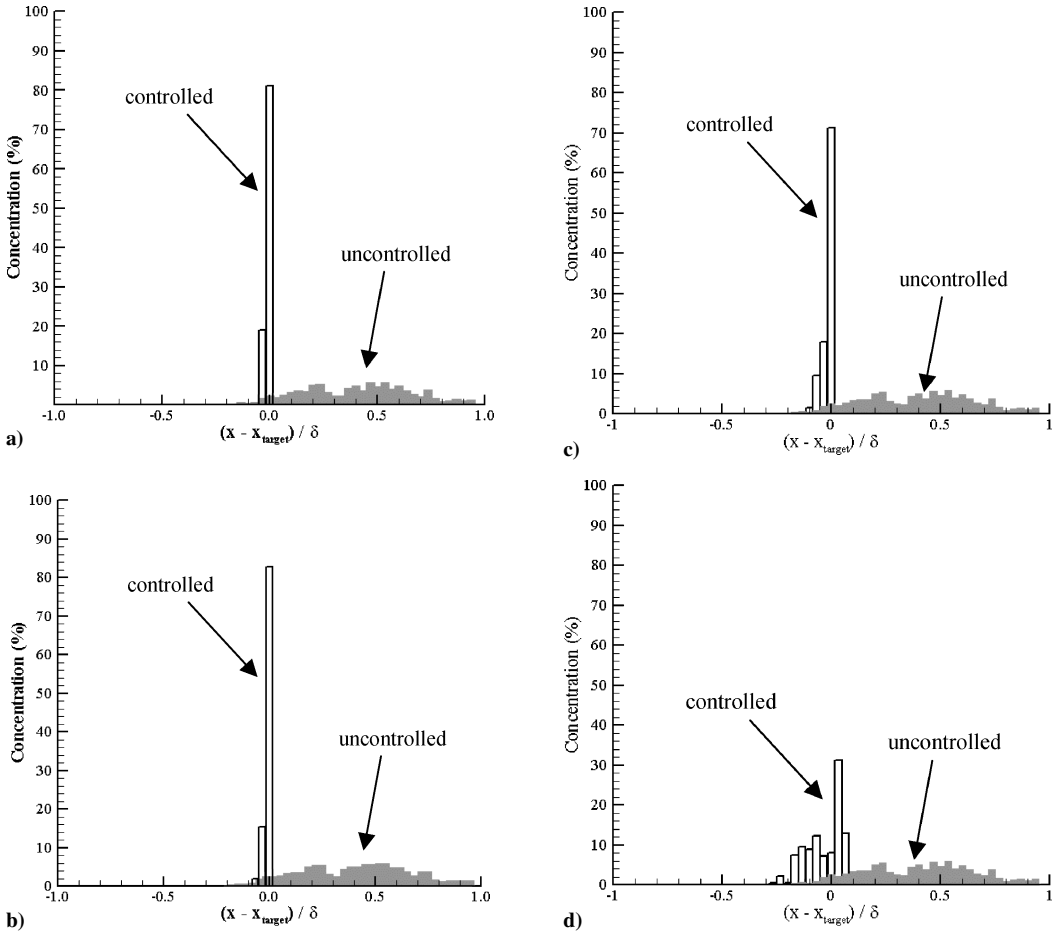

Fig. 9 Probability distribution of vehicle landings for a) vehicles knowing the true mean fluid velocities and vehicles subjected to b) ±10%, c) ±20%, and d) ±50% errors in the mean fluid velocity.

locations at the mean boundary-layer edge was investigated for a fixed target point.

Figure 10 shows scatter plots of the landing locations in the plane of the ground for three selected cases of this study. For $(x_{\text{release}} - x_{\text{target}})/\delta = -3.67$ (Fig. 10a), it is seen that the centroid of the controlled vehicles is much closer to the target than that of the uncontrolled vehicles, but the vehicles appear to spread the same amount in both cases. This is a result of this particular injection condition—the target is almost too far downstream for the controlled vehicles to reach. In this situation, the vehicles will decrease their V_{term} to its minimum value (which corresponds to $\theta = 80$ deg) and travel as far downstream as possible. In this configuration the vehicles are quite susceptible to turbulent dispersion as their relative speed is not large compared to the turbulent fluctuations. In addition, the vehicles are at or near the adaptability limit (near maximum θ) so that the effective dynamic range of control is quite small. Thus, the cloud disperses significantly as is travels towards the target. Figure 10c, $(x_{\text{release}} - x_{\text{target}})/\delta = 0.9$, shows the other extreme, a release point farther downstream than the target location. As the vehicles have no ability to move upstream (recall that no lifting surfaces are included), they have no chance of landing on the target. In this situation the control law still attempts to place the vehicles as close to the target as possible and thus sets the vehicles to their maximum terminal velocity (corresponding to the minimum θ of 10 deg). The controlled vehicles land closer to the target than the uncontrolled vehicles (as in Fig. 10a), but this time the vehicles land at nearly the same streamwise position as the high terminal velocity prevents significant turbulent dispersion. Figure 10b represents an intermediate case between these two extremes and shows that the controlled vehicles can land very near the target x location. The uncontrolled vehicles are reasonably close to the target as well but are substantially spread out as a result of turbulence.

The mean landing and mean-square landing statistics are presented in Fig. 11. Figure 11a shows the results for the mean landing location for various release points. Three data sets are included on this plot: 1) the predicted landing for the uncontrolled vehicle (based on mean-velocity field integrations), 2) the actual uncontrolled landing location (based on the DNS calculations), and 3) the actual controlled vehicle landing locations (based on the DNS calculations). Although the predicted landing locations lie on a straight line (as expected based on a net horizontal movement of about 2δ), it is seen that the actual landing locations do not necessarily coincide with these points and tend to deviate somewhat from the straight line. This can be expected because of the complex structure of the boundary layer and the fact that vehicles are released for a small amount of time and thus tend to see only a few different turbulent structures on their descent to the ground.[15] If many realizations were considered over a very long period of time (approaching infinity), the DNS uncontrolled data and the integrations based on the mean statistic field should provide identical results for the mean landing location. Thus, as already mentioned, the mean field integrations might only be an approximate representation of the mean landing location for the uncontrolled vehicles in the turbulent field.

The uncontrolled vehicle results can be compared to the controlled cases for which the vehicles autonomously adjust the trajectory throughout the flight. In general, the controlled vehicles released from the intermediate points land very near the intended target over a large range of release locations (nearly 4δ). At the extreme release locations one would expect the error in the controlled vehicles' mean landing location to grow linearly as in the uncontrolled case; this is seen clearly for the vehicles released downstream of the target. In these two limits (far upstream and far downstream of the target), the vehicle is essentially uncontrolled as the control law simply imposes either the maximum or minimum terminal velocity

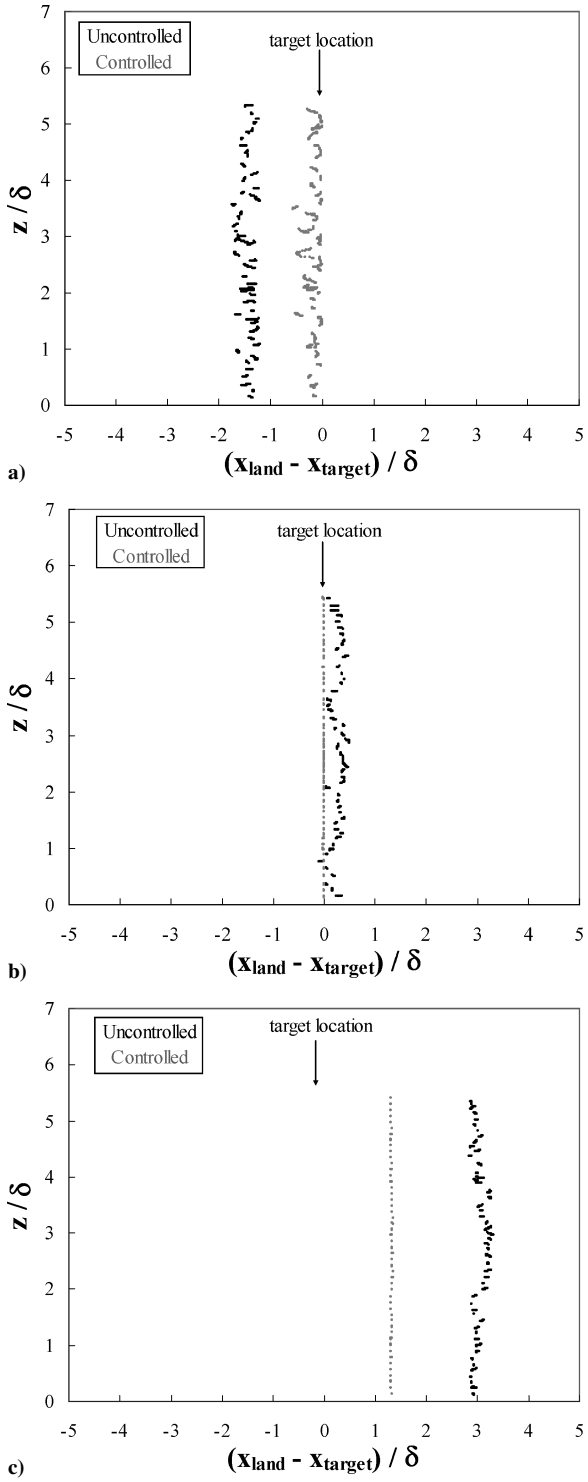

Fig. 10 Vehicle landing positions for controlled and uncontrolled vehicles for $(x_{release} - x_{target})/\delta$ = a) −3.67, b) −1.71, and c) 0.9.

allowed for the configuration in an attempt to place the vehicle as close as possible to the target.

Figure 11b shows the mean-square error in the landing location normalized by the square of the boundary-layer thickness. This error indicates the degree of variance around the target location. Note that in all cases the mean-square error for the controlled vehicles is less than that of the uncontrolled vehicles. This indicates that the controlled vehicles are less dispersed when they land for all release locations considered. Also note that the smallest mean-square error for the controlled vehicle is associated with a release point of approximately δ upstream of the target while an upstream release point of 2δ is best for the uncontrolled case. This difference is a result of the control law working more effectively with higher terminal velocity values, such that the trajectories are less influenced by the wind turbulence.

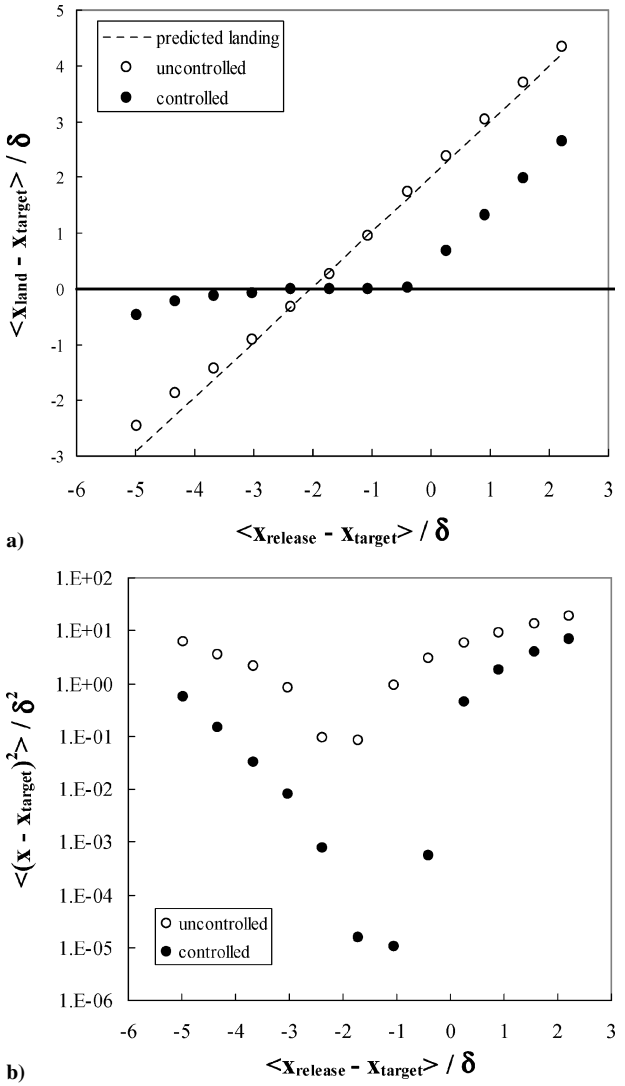

Fig. 11 Statistics for the one-dimensional objective parametric study for a) mean and b) mean-square landing locations.

IV. Conclusions

Trajectory control of terminal-velocity micro air vehicles (modeled as downward-pointing conical structures) in a turbulent atmospheric boundary layer was studied. A direct numerical simulation of the Navier–Stokes equations was employed to model the unsteady, three-dimensional, neutrally stable atmospheric boundary layer. Implementation of a simple control law that uses estimates of a vehicle's trajectory to appropriately vary its terminal velocity showed substantial improvements over uncontrolled vehicle distributions. A second study examined the influence of wind velocity error used for the estimated trajectory calculations. The control law was seen to tolerate as much as a ±50% error in the mean velocity field and still outperform the uncontrolled case. A third study considered a broad range of streamwise release locations, where it was found that a high concentration of vehicles could still be placed on the target streamwise location.

References

[1]Estrin, D. L. (ed.), *Embedded, Everywhere: A Research Agenda for Networked Systems and Embedded Computers*, National Academy Press, Washington, DC, 2001, Chap. 1.

[2]Estrin, D. L., Govindan, R., Heidemann, J. H., and Kumar, S., "Next Century Challenges: Scalable Coordination in Sensor Networks," *Proceedings of MobiCOMM*, Association for Computing Machinery, Special Interest Group on Mobile Computing, New York, 1999, pp. 263–270.

[3]Steere, D., Baptista, A., McNamee, D., Pu, C., and Walpole, J., "Research Challenges in Environmental Observation and Forecasting Systems," *Proceedings of MobiCOMM*, Association for Computing Machinery, Special Interest Group on Mobile Computing, Boston, 2000, pp. 292–299.

[4]Tilak, S., Abu-Ghazaleh, N. B., and Heinzelman, W., "A Taxonomy of Wireless Micro Sensor Network Models," *SIGMOBILE Mobile Computing and Communication Review*, Vol. 6, No. 2, 2002, pp. 28–36.

[5]Howard, A., Mataric, M. J., and Sukhatme, G. S., "Mobile Sensor Network Deployment Using Potential Fields: A Distributed Scalable Solution to the Area Coverage Problem," *Distributed Autonomous Robotic Systems 5*, Springer, Tokyo, 2002, pp. 299–308.

[6]Hoover, A., and Olsen, B. D., "Sensor Network Perception for Mobile Robotics," *Proceedings of IEEE Conference on Robotics and Automation*, Inst. of Electrical and Electronics Engineers, New York, 2000, pp. 342–347.

[7]Cortés, J., Martínez, S., Karatas, T., and Bullo, F., "Coverage Control for Mobile Sensing Networks," *IEEE Transactions on Robotics and Automation*, Vol. 20, No. 2, 2004, pp. 243–255.

[8]Zusmann, E., Yarin, A. L., and Weihs, D., "A Micro-Aerodynamic Decelerator Based on Permeable Surfaces of Nanofiber Mats," *Experiments in Fluids*, Vol. 33, May 2002, pp. 315–320.

[9]Spalart, P. R., and Watmuff, J. H., "Experimental and Numerical Study of a Turbulent Boundary Layer with Pressure Gradients," *Journal of Fluid Mechanics*, Vol. 249, 1991, pp. 337–371.

[10]Dorgan, A. J., and Loth, E., "Simulation of Particles Released near the Wall in a Turbulent Boundary Layer," *International Journal of Multiphase Flow*, Vol. 30, No. 6, 2004, pp. 649–673.

[11]Hinze, J. O., *Turbulence*, McGraw–Hill, New York, 1959, Chap. 7.

[12]Loth, E., "Numerical Approaches to Dilute Two-Phase Flow," *Progress in Energy and Combustion Science*, Vol. 26, No. 3, 2000, pp. 161–223.

[13]White, F. M., *Fluid Mechanics*, 5th ed., McGraw–Hill, New York, 2003.

[14]Dorgan, A. J., "Boundary Layer Dispersion of Near-Wall Injected Particles of Various Inertias," M.S. Thesis, Dept. of Aeronautical and Astronautical Engineering, Univ. of Illinois, Urbana, IL, Dec. 2003.

[15]Bocksell, T. L., "Numerical Simulation of Turbulent Particle Diffusion," Ph.D. Dissertation, Dept. of Aeronautical and Astronautical Engineering, Univ. of Illinois, Urbana, IL, Dec. 2003.

R. So
Associate Editor